Journal of Building Engineering 44 (2021) 103271

Contents lists available at ScienceDirect

Journal of Building Engineering

journal homepage: www.elsevier.com/locate/jobe

Limit analysis of conical and parabolic domes based on semi-analytical solution☆

Renato Zona [a,b,*], Paolo Ferla [a,c], Vincenzo Minutolo [a,d]

[a] Department of Engineering, University of Campania, "L.Vanvitelli" Via Roma, 29, 81031 Aversa, Ce, Italy
[b] Mathematics, Physics, and Engineering Applications Doctorate, Italy
[c] Industrial Engineering Doctorate, Italy
[d] Advisor at Doctorate School, Professor of Structural Engineering, Italy

ARTICLE INFO

Keywords:
Limit analysis
Lower bound theorem
Thrust network
Symmetric domes

ABSTRACT

The evaluation of limit loads of masonry domes has received increasing interest especially due to the importance of historical buildings where domes mainly are one of the most relevant structures. The limit design is used to obtain the safety assessment and the design guidance for restoration and transformation toward preservation and reuse of historical heritage. In the following paper, we present a formulation of the limit analysis based on the semi-analytical approach that starts on Melan's theorem. The self-equilibrated Melan's residual is obtained through the discretization of the analytical form of the equilibrium equation of the spherical dome. The procedure provides a finite-dimensional map of the eigenstress of the structure. Furthermore, the superimposition of the elastic solution to actual loads, obtained by finite element calculation, completes the admissible stress evaluation. Such amissible stress is introduced into the maximization algorithm, based on the lower bound theorem, which results in the collapse load. The same approach is used to get the safety assessment under prescribed load that allows checking the safety of prescribed load pattern and geometry.

1. Introduction

Masonry structures have been widely employed in the past centuries, due to masonry compression strength and long-time durability. Nevertheless, they are still part of a relevant research topic interest, because there are lots of aspects with great research interest nowadays. In fact, despite a strong compression resistance, masonry presents no tensile stress, which makes the study of this construction technique more singular.

Masonry is characterized by many different behaviors that make standard modeling more complex such as anisotropy, heterogeneity, inelastic stress-strain law, and fragile rupture. Moreover, the process analysis has a significant indeterminacy due to complex 3D geometry.

For these considerations and despite the complexity of the problem, the theory of plasticity, namely the limit analysis, can be a useful tool for the evaluation of the safety factor of structures and is widely used to assess the safety level of ancient and historical structures. The primary necessity in the limit analysis context is, therefore, to define the limit domain where to search for stress that does not cause the collapse in the structure.

For these reasons, masonry has been the subject of numerous studies. A rigid-block approach can be found in Refs. [1,2] where masonry structure are studied according to limit equilibrium principles. Many other authors recently proposed a comprhensive study about limit equilibrium and limit analysis of masonry structures [3–6].

The present paper discusses a coupling between numerical and analytical solutions of loaded masonry structures, with reference to conical masonry arches, modeling the structure concerning Limit Analysis [7,8].

Applications of limit analysis for researching the collapse load and, in general, of masonry mechanical behavior can be found in the literature. Franciosi [9] and Breccolotti et al. [10] study the in-plane masonry arch bridges seismic capacity, Tempesta et al. [11] deal with masonry arches safety, and Coccia et al. [12] face cracked masonry portal frames and their in-plane collapse. Ghirlanda et al. determined the collapse behaviour under seismic loads for masonry domes [13,14] For circular masonry arches, static and kinematic approaches have been employed to study collapse induced by external dislocations [15–21]. A discrete

☆ This is a footnote associated with the title.

* Corresponding author. Department of Engineering, University of Campania, "L.Vanvitelli" Via Roma, 29, 81031, Aversa, Ce, Italy.
E-mail address: Renato.zona@unicampania.it (R. Zona).

https://doi.org/10.1016/j.jobe.2021.103271
Received 24 May 2021; Received in revised form 25 August 2021; Accepted 5 September 2021
Available online 11 September 2021

element approach [21,22] can be used to investigate the support settlement. This approach is also employed to study masonry pointed vaults [23]. In Refs. [24,25] the minimum thickness of elliptical masonry arches is analyzed with a static approach.

Aita et al. [26] investigate the load-bearing capacities and the mechanical response of masonry elliptical arches. In the present paper, a methodology for the study of no-tensile strength materials is adopted to evaluate the mechanical behavior both in the linear and nonlinear case. An example of this methodology has been discussed in Ref. [27] for parabolic domes. In the following, the use of spherical analytical solution mixed with FEM analysis for the case of catenary conic-approximated and the parabolic dome is discussed.

2. Materials and method

2.1. Introduction to limit analysis

In this paper, the solution of domes of revolution [27] by using the equation of the shells [28] combined with lower bound theorem and FEM analysis has been described.

A brief introduction of the lower bound theorem and the shell equations are reported as follows, focused on the identification of the relations for the compatibility domain.

Let the structure be subjected to a set of volume and boundary forces $f^n$and p^n, $n \in \{1, 2, \ldots m\}$, a function of time. The mechanical time-depending response consists of the stress σ, and the strain ε. Time is the parameter of the incremental process purely, but no dynamical effects arise on the structure. Moreover, the load intensities belong to a limited domain; it is possible to express the loads' variability by a multiplier k. The structure is made of not-tensile resistant (NTR) elastic-plastic standard material [29]. Namely, the stress-strain constitutive relation links the reversible strain to the stress if the stress belongs to the admissibility domain, K, and relates the permanent strain rate $\dot{\varepsilon}^p$ to the stress when the stress and the stress increment both attain the domain boundary (Eqn 1). As usual, strain energy w and plastic potential π are introduced to formulate the constitutive low, moreover, we assume that the elastic energy and the plastic dissipation at the yield limit were positive.

$$\begin{aligned} &\sigma = \frac{\partial w}{\partial \varepsilon}, \sigma \in \text{interior } (K) \\ &\dot{\varepsilon}^p = \dot{\lambda}\frac{\partial \pi}{\partial \sigma}, \{\sigma, \sigma + d\sigma\} \in \partial \mathrm{K} \\ &\frac{\partial w}{\partial \varepsilon} d\varepsilon \geq 0 \\ &\frac{\partial \pi}{\partial \sigma} d\sigma \geq 0 \end{aligned} \tag{1}$$

The procedure to calculate the limit load multiplier $\dot{\lambda}$ has been based on the lower bound theorem in the form of Melan's theorem that has been formulated for time-variable load history. The time-independent limit load results as a particular case of Melan's theorem provided the actual stress increases monotonically. The solution is found in the space of eigenstress. To the scope, the stress is decomposed as follows (Eqn 2):

$$\sigma = \sigma^e + \sigma^0 \tag{2}$$

Where σ^0 is the eigenstress, i.e., the self-equilibrated stress that has to be superimposed to the perfect elastic stress σ^e to get the actual stress σ. The actual residual stress belongs to the eigenstress set that constitutes the kernel of the equilibrium equation. The actual stress does satisfy the plastic compatibility conditions.

In the following, we have assumed to use a generalized stress formulation where the stress has been described through its resultant and moment acting on the cross-sections of the structural element that has been discussed in detail in the next sections. In the proposed application, only axial and bending stress influence the safety of the structure since shear effects are assumed to be negligible due to the small thickness of the dome.

At first, let us focus our attention on a one-dimensional structure constituting an arc to clarify the procedure.

The rectangular cross-section's dimensions are: h its height and b its width, in the case of a three-dimensional shell, one can take $b = 1$ and consider the stress per unit width. The structure bears distributed load. The internal forces, N, and M, are respectively the resultant and the resultant moment of the stress acting on the section. The forces acting on the cross-section are statically equivalent to a single force of magnitude N applied at the point C that is the center of thrust of the section. The line that connects all the centers of the cross-section along the axis of the structure is called the thrust line.

The compatibility condition for the structure material can be specified through generalized stress considering the inequalities (3):

$$\begin{cases} \frac{N}{bh} - \frac{6M}{bh^2} < 0 \\ \frac{N}{bh} + \frac{6M}{bh^2} < 0 \end{cases} \Leftrightarrow \begin{cases} hN - 6M < 0 \\ hN + 6M < 0 \\ 0 < N \end{cases} \tag{3}$$

The set of inequalities (3) are equivalent to that the center of thrust lays within the core of the cross-section of the arc that is located at the middle third of the section, i.e., $-\frac{h}{6} < \frac{M}{N} < \frac{h}{6}$. These limits correspond to no crack allowed, NCA condition.

A more relaxed condition can be stated whether one admits that in some part in the cross-section the stress vanishes identically, say the section is cracked, although it still works. This latter case corresponds to the fact that the thrust line belongs to the cross-section at least (Eqn 4):

$$\frac{\mathrm{h}}{2} < \frac{\mathrm{M}}{\mathrm{N}} < \frac{\mathrm{h}}{2} \tag{4}$$

So that the compatibility inequalities in (3) can be rewritten as:

$$\begin{cases} hN - 2M < 0 \\ hN + 2M < 0 \\ 0 < N \end{cases} \tag{5}$$

These limits correspond to allowed cracks, CA condition.

Further generalization of the formulation is obtained by comprising the case of tensile resistant materials, TR, $\sigma_y^t \neq 0$. To get this generalization one can modify the right-hand side of the inequalities introducing the upper bound limit of the axial stress (Eqn 6).

$$\mathrm{N}_0 = \sigma_{\mathrm{y}}^{\mathrm{t}} \mathrm{hb} \tag{6}$$

Finally, the compatibility inequation becomes:

$$\begin{cases} \mathrm{hN} - \alpha \mathrm{M} < \beta \mathrm{N}_0 \mathrm{h} \\ \mathrm{hN} + \alpha \mathrm{M} < \beta \mathrm{N}_0 \mathrm{h} \\ \mathrm{N} < \beta \mathrm{N}_0 \end{cases} \tag{7}$$

where

$$\begin{aligned} \alpha &= \begin{cases} 2 & \text{for CA condition} \\ 6 & \text{for } NCAcondition \end{cases} \\ \beta &= \begin{cases} 0 & \text{for NTR materials} \\ N_0 & \text{for } TR \text{ materials} \end{cases} \end{aligned} \tag{8}$$

The drawing in Fig. 1 represents the compatibility domain in N, M plane. The two cases of NTR and the tensile resistant material are represented. In the picture monotone loading cases are represented as a vector N-M. In the NTR case if N-M belongs to the domain, it will remain within the domain even if it is amplified indefinitely. Conversely, in the case of tensile resistant material if the N-M vector has its slope less than $tan\phi$ the same case of NTR occurs, but when the slope of a vector N-M is greater than $tan\phi$, it satisfies the compatibility depending on its magnitude.

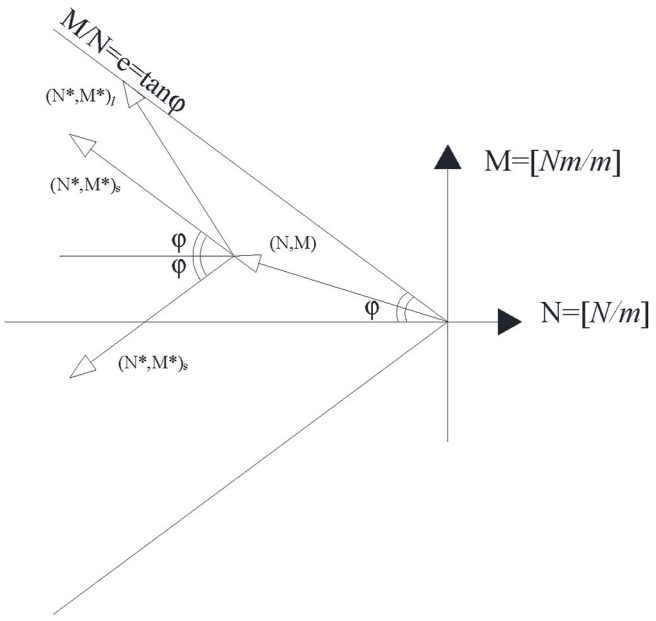

Fig. 1. Compatibility domain.

2.2. Self-equilibrated solutions for domes of revolution

In this section, the equilibrium equations for a dome of revolution have been described. The solution of the homogeneous form of the differential equation formalized in Timoshenko represents the domain of the eigenstress. In this section, the equilibrium equation for the dome of revolution is briefly recalled. Moreover, the equation's specification to spherical domes is presented. The spherical dome model described is aimed to approximate parabolical domes as well by geometrical construction. The procedure can recognize the spherical surface that fits the prescribed parabola and allows applying the spherical equations to parabolas too.

Moreover, the equation of conical domes is derived by a limiting process starting from the equations of spheres.

Let us consider a double curvature dome; to write the equilibrium equations a small element of surface, belonging to the middle plane of the dome, is considered Fig. 2. Sections a-b and c-d represent an infinitesimal portion of two meridian curves, and curves a-c and b-d, are the two parallel ones, that describe a shell of infinitesimal area.

N_i, T_i and M_i are the generalized stresses per unit length, namely axial stress, shear, and bending moment acting on the meridian curves for $i = 1$, and on the parallel for $i = 2$ respectively.

The equilibrium equation of the dome of revolution are the following:

$$\begin{aligned}
&\frac{d(N_1 r)}{d\theta} - N_2 R_1 cos\theta - T_1 r = -XR_1 r \\
&N_1 r + N_2 R_1 sin\theta + \frac{d(T_1 r)}{d\theta} = ZR_1 r \\
&\frac{d(M_1 r)}{d\theta} - M_2 R_1 cos\theta - T_1 R_1 r = 0
\end{aligned} \tag{9}$$

It can be seen that, due to the dome symmetry and cylindrical symmetry of the loads and the structure, the stresses are not dependent on the longitude ϕ so they are functions of the colatitude θ only. equation (9) can be simplified when referred to spherical domes under axially-symmetric loads, the radius r of the parallel curve, indeed, depends on the colatitude as well:

$$r = R_1 sin\theta \tag{10}$$

That substituted into (8) furnishes the equations for spherical domes:

$$\begin{aligned}
&\frac{d(N_1 R_1 sin\theta)}{d\theta} - N_2 R_1 cos\theta - T_1 R_1 sin\theta = -XR_1^2 sin\theta \\
&N_1 R_1 sin\theta + N_2 R_1 sin\theta + \frac{d(T_1 R_1 sin\theta)}{d\theta} = ZR_1^2 sin\theta \\
&\frac{d(M_1 R_1 sin\theta)}{d\theta} - M_2 R_1 cos\theta - T_1 R_1^2 sin\theta = 0
\end{aligned} \tag{11}$$

The solution of equation (10) is sought by the superimposition of the general integral of its associated homogeneous and a particular solution of the inhomogeneous equation. The general integral of the associated homogeneous equation consists of the set of $\{N_1^0, M_1^0, T_1^0, N_2^0, M_2^0\}$ that is the set of the self-equilibrated stress solution of the following equations:

$$\begin{aligned}
&\frac{d(N_1^0 r)}{d\theta} - N_1^0 R_1 cos\theta - T_1^0 r = 0 \\
&N_1^0 r + N_1^0 R_1 sin\theta + \frac{d(T_1^0 r)}{d\theta} = 0 \\
&\frac{d(M_1^0 r)}{d\theta} - M_2^0 R_1 cos\theta - T_1^0 R_1 r = 0
\end{aligned} \tag{12}$$

2.2.1. Parabolic domes

The equations of spherical domes can be extended to parabolic domes of revolution, provided one can approximate the parabolic meridian curve with circumference arc as is briefly explained in Fig. 3. The figure refers to the SMF parabolic dome by Brunelleschi. The circular approximation of the dome middle surface allowed using the equation formulated for the spheres to paraboloids as well. The approximation requires the knowledge of the right geometry, i.e. the radius of the approximating sphere, $R = R_1$, its actual ending and starting angles, α_1

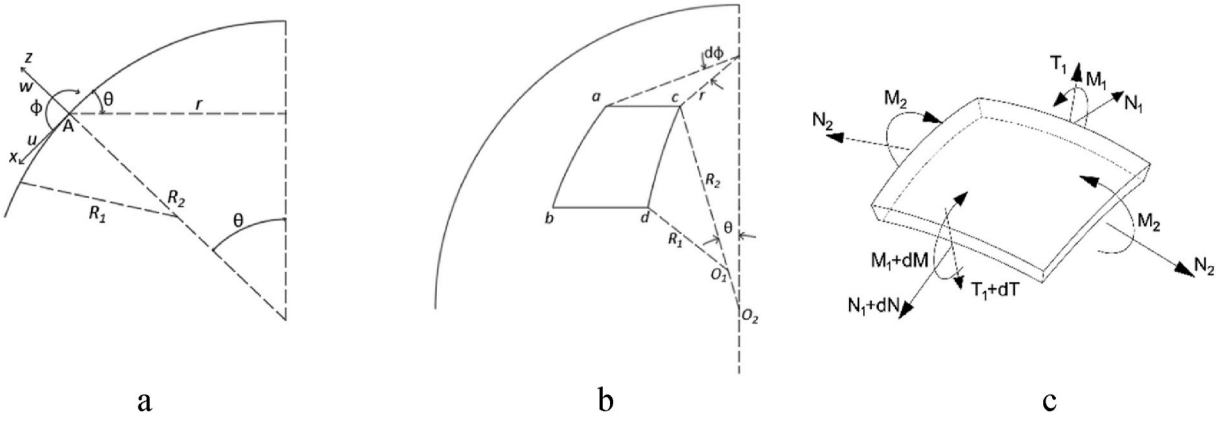

Fig. 2. Geometric parameters (a), an infinitesimal element of the dome (b), and generalized stress on an infinitesimal element (c).

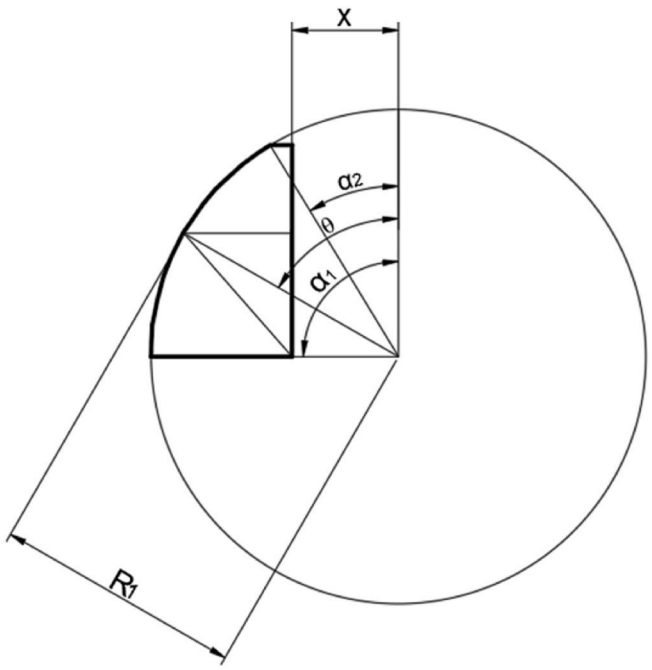

Fig. 3. Parabola to circle approximation.

and α_2, and the position of the revolutionary axis of the dome with respect to the axis of the approximating sphere, x. The approximating circle is obtained through an optimization procedure between the two curves. In the actual case of the Brunelleschi dome, the numerical results have been presented in the next section. Following the proposed approximation, equation (11) are useful to formulate parabolic dome equilibrium.

To get the desired equations one can assume the following expression for the values of the parallel radius:

$$r = R_1 sin\theta - x \tag{13}$$

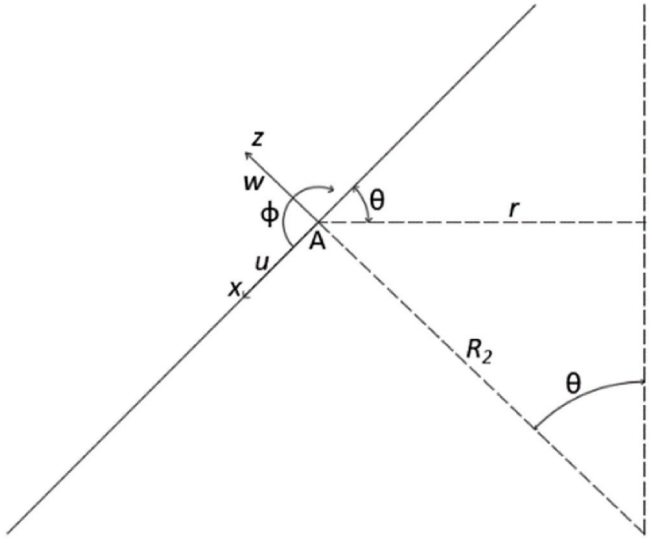

Fig. 4. Conic directrix geometry.

2.2.2. Conical domes

The case of conical domes can be derived starting from equation (8) considering that the curvature radius of the meridian approaches infinity Fig. 4.

The sought equations are formally derived posing $d\theta = dx/R_1$, as an example, the first of (8), modified according to this position is reported hereafter:

$$\frac{d(N_1 r)}{dx}\frac{dx}{R_1}R_1 d\phi - N_2 R_1 cos\theta \frac{dx}{R_1}d\phi - T_1 r cos\theta \frac{dx}{R_1}d\phi = 0 \tag{14}$$

Finally, a limit is taken for $dx/R_1 \to 0$, resulting in:

$$\begin{aligned} &\frac{d(N_1 r)}{dx} - N_2 cos\theta + Xr = 0 - N_2 R_1 sin\theta - \frac{d(T_1 r)}{dx} + Zr = 0 \\ &\frac{d(M_1 r)}{dx} - M_2 cos\theta - T_1 r = 0 \end{aligned} \tag{15}$$

As the last step, one has to highlight the dependence of the mechanical quantities of the colatitude θ in explicit, resulting in the following conical domes equilibrium equations:

$$\begin{aligned} &\frac{d(N_1 r)}{d\theta}\frac{d\theta}{dx} - N_2 cos\theta = 0 - N_2 sin\theta - \frac{d(T_1 r)}{d\theta}\frac{d\theta}{dx} = 0 \\ &\frac{d(M_1 r)}{d\theta}\frac{d\theta}{dx} - M_2 cos\theta - T_1 r = 0 \end{aligned} \tag{16}$$

It has to be recalled that in conical domes the radius of the parallel is a function of the colatitude as well, in particular, the actual radius has the following expression:

$$\mathrm{r}(\theta) = \frac{rmax}{1 + \frac{ctan\theta}{h}(rmax - rmin)} \tag{17}$$

where the maximum radius and the minimum radius are *rmax* and *rmin* respectively and h is the height of the cone.

2.2.3. Numerical discretization

A set of shape functions is used to pursue the numerical approximation of the solution of equation (10). They were part of the set of polynomials of degree n, and depend on the colatitudes angle θ:

$$S_n(\theta) = \left[\theta^0, \theta^1, \ldots, \frac{\theta^n}{n!}\right] \tag{18}$$

To approximate the unknown self-equilibrated stresses, five nodal parameter sets that multiply the shape functions (18) are adopted, leading to iso-parametric representation for all the stress functions.

$$\begin{cases} \boldsymbol{N}_1 = \left[n_{1_0}, n_{1_1}, \ldots, n_{1_i}\right]^T \\ \boldsymbol{N}_2 = \left[n_{2_0}, n_{2_1}, \ldots, n_{2_i}\right]^T \\ \boldsymbol{M}_1 = \left[m_{1_0}, m_{1_1}, \ldots, m_{1_i}\right]^T \\ \boldsymbol{M}_2 = \left[m_{2_0}, m_{2_1}, \ldots, m_{2_i}\right]^T \\ \boldsymbol{T}_1 = \left[t_{1_0}, t_{1_1}, \ldots, t_{1_i}\right]^T \end{cases} \tag{19}$$

The self-equilibrated stresses have been described using coefficients (19), and shape functions (18) by the following matrix form:

$$\begin{cases} N_1^0(\theta) = S_n(\theta)\cdot\boldsymbol{N}_1 \\ N_2^0(\theta) = S_n(\theta)\cdot\boldsymbol{N}_2 \\ M_1^0(\theta) = S_n(\theta)\cdot\boldsymbol{M}_1 \\ M_2^0(\theta) = S_n(\theta)\cdot\boldsymbol{M}_2 \\ T_1^0(\theta) = S_n(\theta)\cdot\boldsymbol{T}_1 \end{cases} \tag{20}$$

The derivatives of these stress functions were:

$$\begin{cases} \dfrac{dN_1^0(\theta)}{d\theta} = dS_n(\theta)\cdot \boldsymbol{N}_1 \\ \dfrac{dN_2^0(\theta)}{d\theta} = dS_n(\theta)\cdot \boldsymbol{N}_2 \\ \dfrac{dM_1^0(\theta)}{d\theta} = dS_n(\theta)\cdot \boldsymbol{M}_1 \\ \dfrac{dM_2^0(\theta)}{d\theta} = dS_n(\theta)\cdot \boldsymbol{M}_2 \\ \dfrac{dT_1^0(\theta)}{d\theta} = dS_n(\theta)\cdot \boldsymbol{T}_1 \end{cases} \tag{21}$$

in which $dS_n(\theta)$ is the matrix of the derivative of the shape functions:

$$\mathrm{dS_n}(\theta) = \left[0, 1, \theta, \ldots, \frac{\theta^{n-1}}{(n-1)!}\right] = [0] \cup \mathrm{S_{n-1}}(\theta) \tag{22}$$

Equations (20)–(22) can be substituted into equations 10 and 11 relating to the equations in discretized form.

Collecting the unknown parameters in a single vector $\boldsymbol{x} = [\boldsymbol{N}_1, \boldsymbol{N}_2, \boldsymbol{M}_1, \boldsymbol{M}_2, \boldsymbol{T}_1]$, self-equilibrium equations can be rewritten in compact matrix form

$$\boldsymbol{A}\boldsymbol{x} = 0 \tag{23}$$

Where, for the spherical domes, $\boldsymbol{A}$ is a function of the angle θ, and its explicit expression is the following:

$$\boldsymbol{A}(\theta) = \begin{bmatrix} \left(\dfrac{dr}{d\theta}S_n(\theta) + rdS_n(\theta)\right) & -S_n(\theta)R_1\cos\theta & 0 & 0 & -rS_n(\theta) \\ S_n(\theta)r & S_n(\theta)R_1\sin\theta & 0 & 0 & \left(\dfrac{dr}{d\theta}S_n(\theta) + rdS_n(\theta)\right) \\ 0 & 0 & \left(\dfrac{dr}{d\theta}S_n(\theta) + rdS_n(\theta)\right) & -S_n(\theta)R_1\cos\theta & -rR_1S_n(\theta) \end{bmatrix} \tag{24}$$

Equation (23) has no unique solution since the number of the unknowns is greater than the number of equations. Then it is possible to find only three of the unknown variables as a function of the $5n-3$ leftover ones.

To the scope, matrix A is partitioned into two sub-matrices: a non-singular square matrix B, which rank is 3, and a remaining part C ($3 \times 5n-3$). Accordingly to the matrix partition, the vector x can be divided into a part, b, of dimension 3, and a complementary part c.

The discrete form of the equilibrium equation becomes:

$$[\boldsymbol{B} \quad \boldsymbol{C}]\begin{bmatrix}\boldsymbol{b}\\ \boldsymbol{c}\end{bmatrix} = 0 \tag{25}$$

equation (25), solved for b, gives:

$$\boldsymbol{b} = \boldsymbol{K}\boldsymbol{c} \tag{26}$$

where

$$\boldsymbol{K} = -\boldsymbol{B}^{-1}\boldsymbol{C} \tag{27}$$

The solution of Equation (26) gives the set of all the self-equilibrated stresses as a function of the parameter's vector c, in fact the vector x assumes the form

$$x = \frac{\boldsymbol{K}}{\boldsymbol{I}}\, c \tag{28}$$

The solution of (28) can be substituted in the representation of stress giving the following formal expressions, that highlights the dependence of equilibrated stress on the parameter c.

$$\begin{aligned} \boldsymbol{N}_1 &= \boldsymbol{K}_{N1}\boldsymbol{c} \\ \boldsymbol{N}_2 &= \boldsymbol{K}_{N2}\boldsymbol{c} \\ \boldsymbol{M}_1 &= \boldsymbol{K}_{M1}\boldsymbol{c} \\ \boldsymbol{M}_2 &= \boldsymbol{K}_{M2}\boldsymbol{c} \\ \boldsymbol{T}_1 &= \boldsymbol{K}_{T1}\boldsymbol{c} \end{aligned} \tag{29}$$

2.3. Elastic solution by FEM calculation

Together with the self-equilibrated stress, the proposed procedure requires knowledge of the elastic response of the structure to the applied load pattern. The analytical solution exists only for a few simple cases, consequently, numerical one is reached using Finite Elements through the commercial code Ansys. The elastic solution is collected in the matrix of elastic stresses containing the elastic parameters $\boldsymbol{F}^* = \{\boldsymbol{N}_i^e, \boldsymbol{M}_i^e, \boldsymbol{T}_i^e\}$ referring to a meridian curve. The elastic results have been superimposed to the self-equilibrated ones leading to the optimal program that has furnished the sought safety assessment of the structure.

As previously quoted a twofold strategy has been pursued to get either the safety factor of an assigned load pattern or assessment of a prescribed load pattern where the load factor is assigned in advance. Both the procedures result in a linear programming algorithm provided to consider the suitable objective function. The first being the safety factor, the second being the trust line distance from the middle of the cross-section of the dome shell.

2.3.1. Load multiplier evaluation

The limit multiplier of prescribed load paths, either monotonically increasing or randomly variable, is obtained by maximizing the load multiplier under the constraint that the sum of elastic response, plus any self-equilibrated time-independent stress solution of (22), as a function of c, belongs to the admissible domain. Hence it results that the optimization program has the load multiplier as objective function and the parameters c as variables. The optimization constraints are the linear inequalities representing the limit domain in terms of c.

At first elastic solution is obtained employing FEM analysis. The vectors N_i^e, M_i^e collected the effective generalized stress where $i \in \{1, 2\}$ referred to the meridians or parallel direction, respectively. Collocating the equations at discrete angles, i.e., at a finite number of θ_j with $j \in \{1, \ldots\ldots, m\}$, where m was the number of points along the meridian curve, one gets the solution numerically gives the discretized form of Equation (29):

$$\begin{cases} \mathbf{N}_1^{\mathrm{j}} = \mathbf{K}_{\mathrm{N_1}}^{\mathrm{j}} c \\ \mathbf{N}_2^{\mathrm{j}} = \mathbf{K}_{\mathrm{N_2}}^{\mathrm{j}} c \\ \mathbf{M}_1^{\mathrm{j}} = \mathbf{K}_{\mathrm{M_1}}^{\mathrm{j}} c \\ \mathbf{M}_2^{\mathrm{j}} = \mathbf{K}_{\mathrm{M_2}}^{\mathrm{j}} c \\ \mathbf{T}_1^{\mathrm{j}} = \mathbf{K}_{\mathrm{T_1}}^{\mathrm{j}} c \end{cases} \tag{30}$$

where the superscript $()^j$ referred to the discrete angles θ_j.

Finally, the optimization program, starting from equation (7) has the following discretized form where the stress components, N_i^r and M_i^r, must be calculated via (30)

$$\sup_{c}\left|k\in\mathbb{R}^{+}:\begin{cases}h\left(N_i^r+kN_i^e\right)+\alpha\left(M_i^r+kM_i^e\right)<\beta h\\ h\left(N_i^r+kN_i^e\right)-\alpha\left(M_i^r+kM_i^e\right)<\beta h\\ \left(N_i^r+kN_i^e\right)<\beta\end{cases}\right|^{j} \tag{31}$$

depending on the presence of tensile resistance σ_0 such that axial limit stress is $N_0=\sigma_0 h$ following the material constitutive properties equations (3), (5) and (7).

2.3.2. Safety assessment for prescribed load multiplier

Following the same reasoning, one can state a second optimization program based on the same constraint inequalities (31). The second optimization program evaluates the safety of a prescribed load multiplier. Namely, for a prescribed load factor k, it searched if there exist any self-equilibrated stresses, N_i^r and M_i^r, such that the constraint equations hold. In this latter case, the formulation yield to a constrained minimum program, the objective function being the norm, $\wp$, of the difference between the actual eccentricity $e_{ij}=\left(\frac{M_i}{N_i}\right)_j$ and the limit eccentricity $\frac{h}{2}$ that corresponds to the stresses that violate the equilibrium and compatibility conditions. The resulting formulation has consisted of:

$$\min_{c}\wp\left|\wp\in\mathbb{R}^{+},\wp=\sqrt{\sum_{j=1,m}\left[\sum_{i=1,2}\left(\frac{M_i^r+kM_i^e}{N_i^r+kN_i^e}-\frac{h}{2}\right)^{j}\right]^{2}}:\begin{cases}h\left(N_i^r+kN_i^e\right)+2\left(M_i^r+kM_i^e\right)<\alpha\\ h\left(N_i^r+kN_i^e\right)-2\left(M_i^r+kM_i^e\right)<\alpha\\ \left(N_i^r+kN_i^e\right)<\beta\end{cases}\right|^{j} \tag{32}$$

2.4. General formulation

The procedure has been applied to two actual domes. In particular, the Santa Maria del Fiore (SMF) dome, by Brunelleschi in Florence and the inner vault of Saint Paul (SP) dome in London have been considered. The SMF dome is constituted by two structures, the first is the outer vault made of masonry that is connected to an inner vault made of masonry as well. Both the structures are interconnected and behave as a unicum. The proposed model is applied to an equivalent structure made of a single layer that is assumed to be equivalent to the double layer structure's thickness.

The SP dome is formed by three vaults, the outer is the external structure visible from the street, a second inner vault is the one that can be seen from the interior of the church. Both these vaults have the principal responsibility to give the aesthetical, visual, quality of the dome. The load-bearing capacity is reserved for the middle structure that has the shape of the catenary and has been derived from Hooke's considerations. The procedure proposed is applied to the middle dome that is seen to be described with good approximation with a cone.

For both the analyzed structures, the self-equilibrated solution has been formulated through the numerical procedure that is described in equation (31). The actual elastic solution has been obtained through finite elements using the code ANSYS©.

In Fig. 6, the scheme of the domes is reported and the relevant dimensions of the structures are indicated. The geometry has been used both to resolve equations (11) and (16) and to get the finite element solutions.

As explained in the previous section, for the application of Melan's Theorem, an elastic solution is needed. The closed-form analytic solution exists only for the simple case. For complex load conditions, numerical analysis is more suitable. Numerical analysis can be pursued by FEM for the elastic solution.

2.4.1. Statement of the problem

Two procedures have been stated, the first, Collapse Search Procedure (CSP), evaluated the load collapse multiplier lower-bound by maximization of the statically admissible stress. The second procedure, Safety-Evaluation Procedure (SEP), evaluated the safety of the structure under the load level indicated through a prescribed multiplier k_p.

The load program consisted of the first step with only the self-weight of the structure, dead load. Then, another load step has consisted of a line load acting on a generic parallel of the dome, the accidental load.

At first, the dead load is ramped through the kd parameter that is the load intensity multiplier. Furthermore, ramped accidental load affected by the multiplier ka is superimposed to the dead load at a prescribed nominal level corresponding to kd = 1.

2.4.2. CSP formulation

The calculation is aimed at the research of the collapse value of k, say sc, as the maximum k, for which the compatibility conditions hold.

The routine for the analytical part of the procedure has been compiled through the software Mathematica© [30].

The calculation, concerning only a meridian curve of the dome due to axial-symmetry of the problem, prevised to discretize the meridian by dividing it into 20 segments, see Fig. 5, where to collocate the compatibility inequalities and to calculate the elastic solution.

The self-weight collapse multiplier resulted by the following linear program:

$$\sup_{(N^r,M^r)}k_a\left|\begin{cases}h\left(N_i^r+k_aN_i^e\right)-2\left(M_i^r+k_aM_i^e\right)<\alpha\\ h\left(N_i^r+k_aN_i^e\right)-2\left(M_i^r+k_aM_i^e\right)<\alpha\\ \left(N_i^r+k_aN_i^e\right)<\beta\end{cases}\right|_{j} \tag{33}$$

In the program (33), the elements of vectors N_i^r and M_i^r are the residuals self-equilibrated stresses, the N_i^e and M_i^e are the dead load stress results.

The collapse multiplier of the actual load is the obtained trough the following program

$$\sup_{(N^r,M^r)}k\left|\begin{cases}h\left(N_i^r+N_i^e+kN_i^a\right)+2\left(M_i^r+M_i^e+kM_i^a\right)<\alpha\\ h\left(N_i^r+N_i^e+kN_i^a\right)-2\left(M_i^r+M_i^e+kM_i^a\right)<\alpha\\ \left(N_i^r+N_i^e+kN_i^a\right)<\beta\end{cases}\right|_{j} \tag{34}$$

where N_i^a and M_i^a are the axial stresses and the bending moments due to the accidental loads.

2.4.3. SEP formulation

The SEP refers to evaluating the safety of a prescribed load level. The objective function of the corresponding linear program depended on the design variables, (N_i^r, M_i^r) as in CSP. The load is subjected to the prescribed multiplier λ, and the procedure aims to assess the safety of such a load level. The statement of the problem consists of constrained optimum research where the objective function is the eccentricity of the thrust line which is assumed in the form of equation (35). The

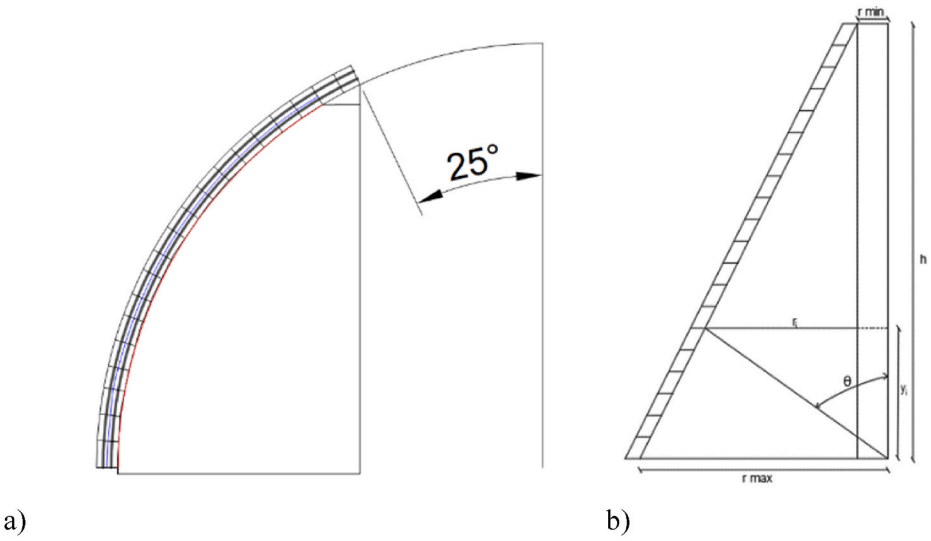

Fig. 5. Dome discretization along meridian: a) SMF; b) SP.

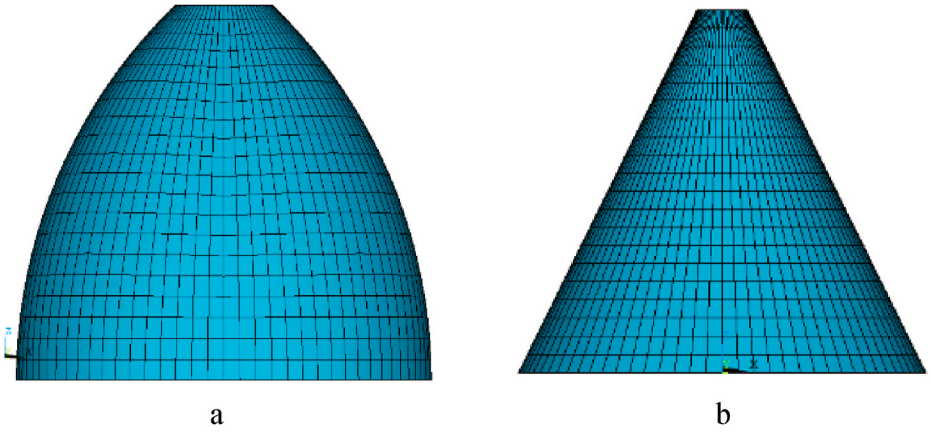

Fig. 6. Finite element models of SMF (a) and SP (b) domes.

constraints of the program are equal to equation (34) provided one assumes $k = \lambda$. The statement of the program is summarized in the following-

$$\min_{(N^r,M^r)} \wp \left| \wp \in \mathbb{R}^+, \begin{cases} h\left(N_i^r + N_i^e + \lambda N_i^a\right) + 2\left(M_i^r + M_i^e + \lambda M_i^a\right) < \alpha \\ h\left(N_i^r + N_i^e + \lambda N_i^a\right) - 2\left(M_i^r + M_i^e + \lambda M_i^a\right) < \alpha \\ \left(N_i^r + N_i^e + \lambda N_i^a\right) < \beta \end{cases}^j \right. \tag{35}$$

Where

$$\wp = \sqrt{\sum_{j=1,m} \left[\sum_{i=1,2} \left(\frac{M_i^r + M_i^e + \lambda M_i^a}{N_i^r + N_i^e + \lambda N_i^a} - \frac{h}{2} \right)^j \right]^2} \tag{36}$$

2.5. FEM elastic solution

FEM model and results have been obtained with ANSYS© software, Fig. 6. The domes have been modeled using four-node shell elements representing the middle surface of the dome and returned the axial forces and bending moments acting along the parallel and the meridian direction.

The base circumference of the structure has been constrained for all the degrees of freedom; so that the base of the dome can be considered clamped. The following load cases have been considered for the analysis:

- o (1) self-weight applied as density and uniform line load applied on the top parallel in the vertical direction that represents the dome's top lantern.
- o (2) uniform line load in radial outward, (3) inward and (4) vertical direction applied on a parallel corresponding to the angle θ_p, $p\{5, 10, 15\}$.The mechanical properties of the structure are reported in the following Table 1:

Table 1
Mechanical properties of the dome.

Young modulus$[N/m^2]$	Poisson's ratio	Weight$[N/m^3]$
18000	0.27	18000

In appendix are contained the results of the elastic analysis used into the Mathematica© notebook to perform the optimization program:

3. Results and discussion

The CSP optimization program gave the limit multiplier and the residual stress at the incoming collapse of the structure. The existence of a residual able to satisfy, together with the actual elastic response, the compatibility constraints is the sufficient condition for the collapse did not occur although the so find residual does not represent the actual

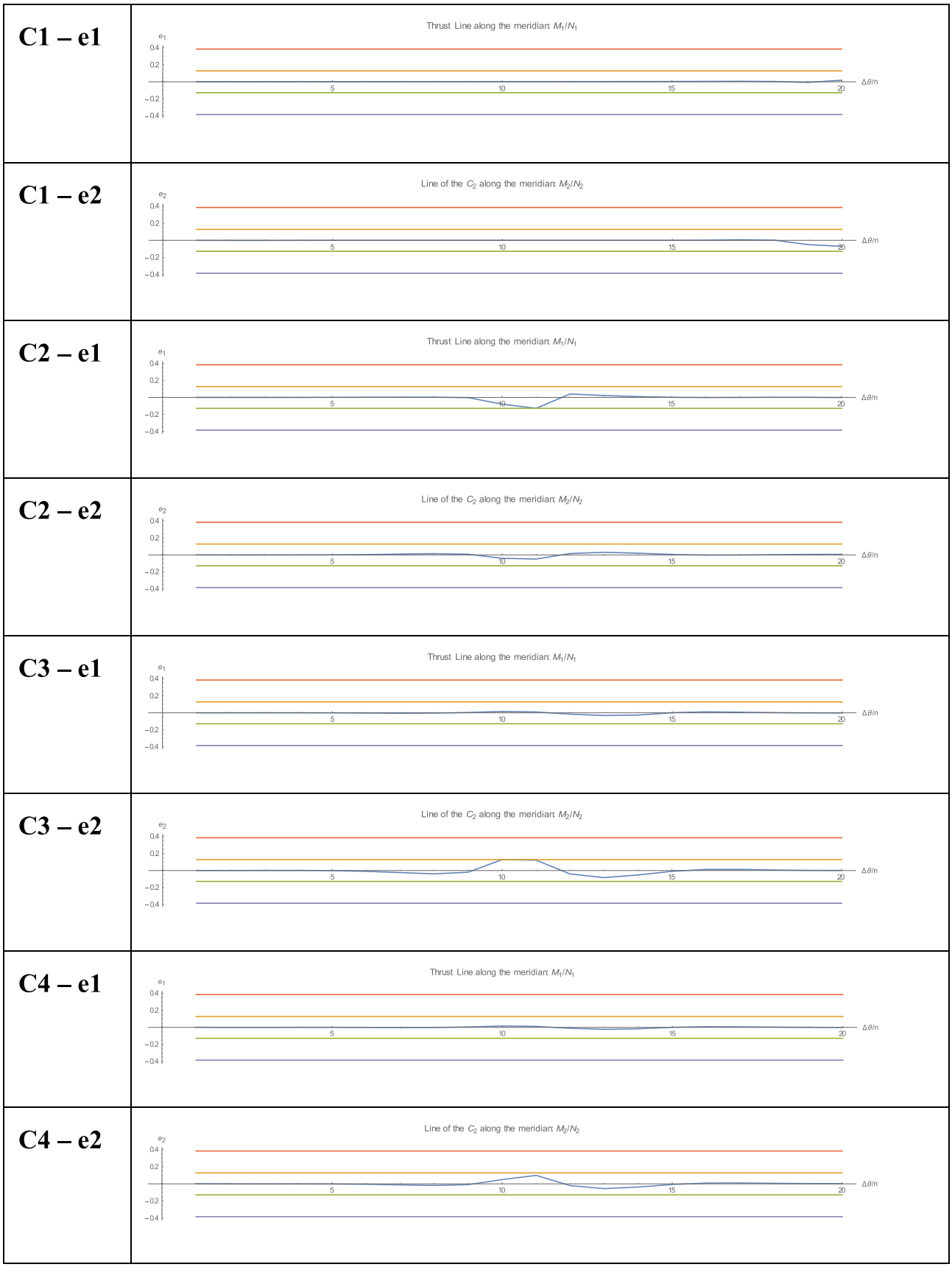

Fig. 7. Thrust line inside sections (SMF) black line, the green and orange lines represent the section core limits, the section thickness is 0.77 m. (For interpretation of the references to colour in this figure legend, the reader is referred to the Web version of this article.)

C1 – e1	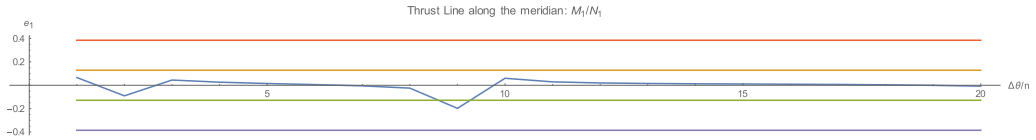
C1 – e2	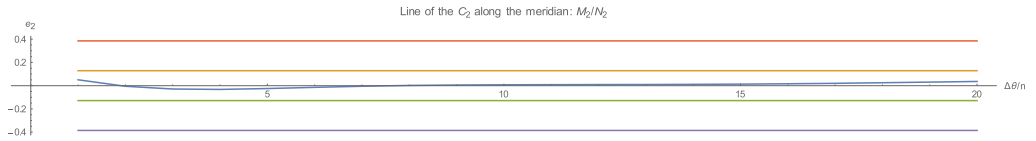
C2 – e1	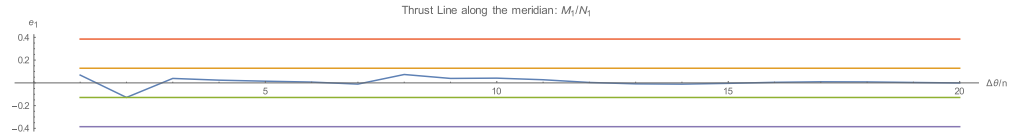
C2 – e2	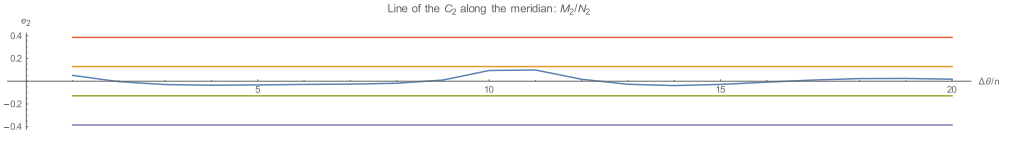
C3 – e1	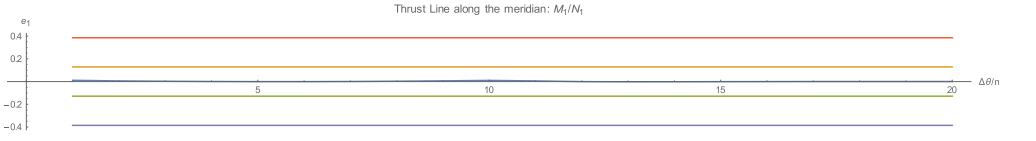
C3 – e2	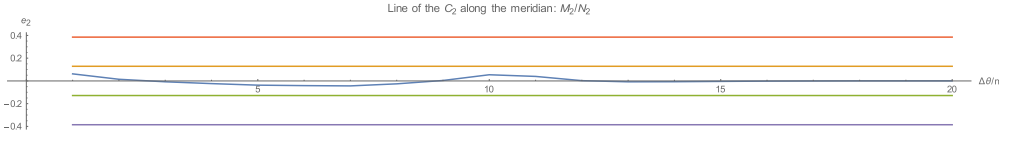
C4 – e1	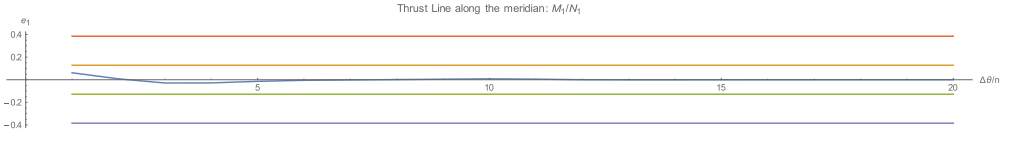
C4 – e2	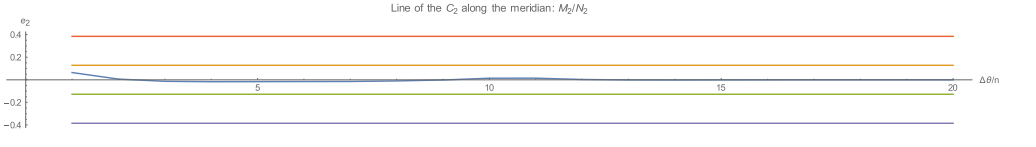

Fig. 8. Thrust line inside sections (SP).

Table 2
Load Multiplier Value comparison.

Load Multiplier	FEM - ANALYTIC	Fem	Ratio
SMF -C1	608.34	615.33	1.01
SP – C1	28.27	31.35	1.10
SMF -C2	29.37	28.77	0.97
SP – C2	2.78	3.12	1.12
SMF -C3	26.58	28.77	1.08
SP – C3	2.36	3.12	1.32
SMF -C4	288.78	311.44	1.07
SP – C4	277.65	297.65	1.07

residual one that we can find in the structure during its life. The CSP allows finding one of the compatible residuals that guarantee the structure safety under the applied loads provided it is amplified by a multiplier less than the obtained collapse one. The output of the CSP is represented by the eccentricity of the axial force both on the parallel oriented and the meridian oriented cross-section of the dome. The eccentricity is plotted along the meridian since it is constant with the longitude.

The figures highlight that the eccentricity is contained within the section thickness which is the compatibility requirement imposed by the program's constraints. A three-dimensional representation of the lines of the centers of axial forces along parallels and meridians should be considered as a thrust network.

Melan's residuals were not the actual ones but those arising from the routine. However, the stress resulted from the calculation is one of the possible statically admissible stress. Fig. 7 and Fig. 8 reported the thrust line along the structure's abscissa respectively for SMF and SP, along the meridian and the parallel directions, named with e1 and e2. The diagrams showed that the calculated thrust line belongs to the structural thickness almost everywhere in the structure. Only in a few points, the thrust line attains the cross-section boundary that confirms that the structure attains the limit at a certain point without collapsing. One can interpret the violation of the limit as the occurrence of a plastic hinge at the point.

In the following Table 2 the benchmark with classic FEM results is reported.

4. Conclusions

In the paper, a semi-analytical method has been described to assess the masonry domes' stability. The method starts from the numerical approximation of the null space of the equilibrium equations of the spherical domes and implements the static approach to limit analysis in a two-way mode. In a first strategy, the safety factor for the prescribed load pattern is obtained through a limiting process accordingly to Melan's theorem. The second strategy has been devoted to evaluating the existence of a statically compatible stress state under prescribed load intensity.

The latter approach consists of the research of admissible stress under prescribed loads that results in an admissible thrust line contained into the structure thickness. The method, in this second way, approaches the thrust line method proposed by Bloch [15].

The formulation is limited to axial-symmetrical domes since it is based on the approximated solution of the closed-form equations of self-equilibrium of the dome. The method can be easily extended to other dome shapes provided the equation expression exists to be solved via the proposed approximation.

For the analyzed cases, the diagram of the resulting eccentricity along the meridian curve of the dome showed that a thrust line can be found that is contained within the dome's thickness. The found solution does guarantee the safety of the investigated structure even if does not represent the actual response of the structure.

Declaration of competing interest

The authors declare that they have no known competing financial interests or personal relationships that could have appeared to influence the work reported in this paper.

Acknowledgements

This research was funded by the Università degli Studi della Campania "L.Vanvitelli", grant Programma VALERE: "VAnviteLli pEr la RicErca", DDG n. 516–May 24, 2018.

Appendix A. Supplementary data

Supplementary data to this article can be found online at https://doi.org/10.1016/j.jobe.2021.103271.

Appendix

Table 3
Numerical Value of stress vector (SMF)

SMF: Self-Weight + Lantern				
ELEM	N_2	N_1	M_2	M_1
1	−43.92	−196.21	−3433.9	−12777
21	−17.76	−183.71	286.91	768.93
41	9.329	−171.66	1717.7	6007.8
61	26.779	−160.33	1785.1	6438.5
81	33.036	−149.79	1245.1	4771.2
101	30.596	−139.98	581.92	2674.8
121	22.948	−130.78	34.249	950.56
141	13.077	−122.02	−326.7	−170.85
161	2.9757	−113.56	−520.15	−756.82
181	−6.2939	−105.32	−598.77	−981.26
201	−14.327	−97.2	−615.11	−1016
221	−21.082	−89.148	−606.82	−985.3
241	−26.653	−81.098	−593.69	−958.5
261	−31.13	−72.975	−580.39	−959.82
281	−34.526	−64.682	−560.34	−980.76
301	−36.792	−56.084	−519.1	−986.43
321	−37.862	−47.004	−436.42	−913.42

(*continued on next page*)

Table 3 (*continued*)

SMF: Self-Weight + Lantern				
ELEM	N_2	N_1	M_2	M_1
341	−37.949	−37.123	−296.94	−671.36
361	−38.033	−25.818	−121.32	−202.69
381	−41.557	−11.038	−63.902	69.371

Table 4
Numerical Value of stress vector (SMF)

Radial inward load				
ELEM	N_2	N_1	M_2	M_1
1	−1.67E-02	−3.51E-04	8.9586	33.705
21	−7.62E-02	−6.46E-04	4.6174	19.464
41	−1.73E-01	2.71E-04	−2.2304	−3.519
61	−2.63E-01	3.96E-03	−13.62	−45.173
81	−2.83E-01	−1.34E-02	−13.226	−46.807
101	−2.16E-01	−9.38E-03	−1.5643	−7.1739
121	−1.28E-01	−5.03E-03	3.6711	10.955
141	−5.60E-02	−1.64E-03	4.7509	15.223
161	−1.08E-02	3.61E-04	3.7778	12.615
181	1.08E-02	1.13E-03	2.2126	7.9067
201	1.64E-02	1.07E-03	0.8536	3.6765
221	1.38E-02	6.38E-04	−1.27E-02	0.86939
241	8.58E-03	1.56E-04	−0.40127	−0.52154
261	3.84E-03	−1.87E-04	−0.45841	−0.90856
281	7.43E-04	−3.36E-04	−0.34783	−0.76233
301	−7.04E-04	−3.23E-04	−0.19483	−0.44442
321	−1.01E-03	−2.16E-04	−7.06E-02	−0.16414
341	−7.48E-04	−8.63E-05	3.13E-04	−2.50E-03
361	−3.14E-04	1.39E-05	2.48E-02	4.15E-02
381	1.93E-04	3.17E-05	2.77E-02	1.98E-02

Table 5
Numerical Value of stress vector (SMF)

Radial outward load				
ELEM	N2	N1	M2	M1
1	1.67E-02	3.51E-04	−8.9586	−33.705
21	7.62E-02	6.46E-04	−4.6174	−19.464
41	1.73E-01	−2.71E-04	2.2304	3.519
61	2.63E-01	−3.96E-03	13.62	45.173
81	2.83E-01	1.34E-02	13.226	46.807
101	2.16E-01	9.38E-03	1.5643	7.1739
121	1.28E-01	5.03E-03	−3.6711	−10.955
141	5.60E-02	1.64E-03	−4.7509	−15.223
161	1.08E-02	−3.61E-04	−3.7778	−12.615
181	−1.08E-02	−1.13E-03	−2.2126	−7.9067
201	−1.64E-02	−1.07E-03	−0.8536	−3.6765
221	−1.38E-02	−6.38E-04	1.27E-02	−0.86939
241	−8.58E-03	−1.56E-04	0.40127	0.52154
261	−3.84E-03	1.87E-04	0.45841	0.90856
281	−7.43E-04	3.36E-04	0.34783	0.76233
301	7.04E-04	3.23E-04	0.19483	0.44442
321	1.01E-03	2.16E-04	7.06E-02	0.16414
341	7.48E-04	8.63E-05	−3.13E-04	2.50E-03
361	3.14E-04	−1.39E-05	−2.48E-02	−4.15E-02
381	−1.93E-04	−3.17E-05	−2.77E-02	−1.98E-02

Table 6
Numerical Value of stress vector (SMF)

Vertical Load				
ELEM	N2	N1	M2	M1
1	−3.08E-02	−0.12969	−0.98313	−3.6274
21	−2.46E-02	−0.1309	1.3564	5.125
41	−2.65E-02	−0.13237	1.4826	5.9605
61	−3.92E-02	−0.13399	−0.66183	−1.6481
81	−1.37E-02	2.90E-04	−1.7352	−5.8001
101	−1.49E-02	7.30E-05	−0.70372	−2.4001
121	−1.14E-02	1.20E-04	−8.28E-02	−0.33957
141	−6.78E-03	2.18E-04	0.19643	0.59603
161	−3.00E-03	3.00E-04	0.25379	0.80881
181	−6.21E-04	3.22E-04	0.20168	0.66339
201	5.00E-04	2.93E-04	0.11867	0.41135
221	7.89E-04	2.30E-04	4.74E-02	0.18791
241	6.49E-04	1.59E-04	2.73E-03	4.19E-02
261	3.80E-04	9.51E-05	−1.65E-02	−2.86E-02
281	1.41E-04	4.85E-05	−1.85E-02	−4.64E-02
301	−5.17E-06	2.00E-05	−1.24E-02	−3.73E-02
321	−6.54E-05	6.54E-06	−4.87E-03	−2.04E-02
341	−6.70E-05	2.48E-06	5.06E-04	−6.88E-03
361	−4.09E-05	2.97E-06	2.86E-03	−3.96E-04
381	−8.28E-07	2.04E-06	3.43E-03	5.28E-04

Table 7
Numerical Value of stress vector (SP)

Self-Weight + Lantern				
ELEM	N_2	N_1	M_2	M_1
1	−239632	−99216.6	56.58386	−48.9512
21	−228518	−93807.3	106.6611	−48.3104
41	−217424	−88814.4	55.55982	−63.5518
61	−206331	−84196.4	−18.6027	−79.9153
81	−195224	−79810.8	−75.9512	−90.8483
101	−184091	−75518.7	−106.183	−95.5197
121	−172924	−71231.2	−115.005	−95.8217
141	−161718	−66911.6	−112.74	−94.1058
161	−150466	−62558.4	−107.763	−92.024
181	−139160	−58184.7	−104.427	−90.2786
201	−127789	−53803.9	−103.721	−88.8701
221	−116334	−49423.9	−104.856	−87.4697
241	−104771	−45047.7	−106.657	−85.6986
261	−93066.7	−40677.5	−108.576	−83.2726
281	−81166.7	−36317.9	−112.107	−80.0553
301	−68990	−31965.1	−122.911	−75.8445
321	−56408.7	−27558.7	−147.112	−68.8823
341	−43218.7	−22942	−154.489	−52.0859
361	−29017.5	−18351.7	−12.76	−19.3532
381	−12514.4	−16216.6	86.5747	−21.8498

Table 8
Numerical Value of stress vector (SP)

Radial outward load				
ELEM	N_2	N_1	M_2	M_1
1	−22.1232	−16.2412	29.5493	3.78262
21	−19.8535	−125.888	92.1551	10.336
41	−5.58613	−495.547	133.974	10.9465
61	39.4784	−1258.14	92.6006	−1.56652
81	138.34	−2281.81	−158.75	−38.4705
101	290.184	−2685.95	−788.3	−107.012
121	395.101	−121.729	−1833.74	−184.055
141	115.412	9537.04	−2709.73	−162.741
161	−1250.52	29839.7	−1288.41	207.513
181	−4488.6	53756.3	6905	1263.82
201	5032.49	58148.8	7127.95	757.76
221	1408.15	33758.2	−2087.54	−875.901
241	−501.295	8500.8	−3696.31	−904.078

(*continued on next page*)

Table 8 (*continued*)

Radial outward load				
ELEM	N_2	N_1	M_2	M_1
261	−817.712	−3506.33	−2059.38	−397.226
281	−422.639	−4637.62	−367.479	−11.6036
301	−33.2474	−1893.58	310.952	100.909
321	100.253	128.591	259.303	58.423
341	58.7329	502.638	48.0539	2.2905
361	−3.65277	151.565	−37.7802	−13.1107
381	−13.6865	−89.8982	−20.2002	−4.344

Table 9
Numerical Value of stress vector (SP)

Radial inward load				
ELEM	N_2	N_1	M_2	M_1
1	22.1232	16.2412	−29.5493	−3.78262
21	19.8535	125.888	−92.1551	−10.336
41	5.58613	495.547	−133.974	−10.9465
61	−39.4784	1258.14	−92.6006	1.56652
81	−138.34	2281.81	158.75	38.4705
101	−290.184	2685.95	788.3	107.012
121	−395.101	121.729	1833.74	184.055
141	−115.412	−9537.04	2709.73	162.741
161	1250.52	−29839.7	1288.41	−207.513
181	4488.6	−53756.3	−6905	−1263.82
201	−5032.49	−58148.8	−7127.95	−757.76
221	−1408.15	−33758.2	2087.54	875.901
241	501.295	−8500.8	3696.31	904.078
261	817.712	3506.33	2059.38	397.226
281	422.639	4637.62	367.479	11.6036
301	33.2474	1893.58	−310.952	−100.909
321	−100.253	−128.591	−259.303	−58.423
341	−58.7329	−502.638	−48.0539	−2.2905
361	3.65277	−151.565	37.7802	13.1107
381	13.6865	89.8982	20.2002	4.344

Table 10
Numerical Value of stress vector (SP)

Radial inward load				
ELEM	N_2	N_1	M_2	M_1
1	−249.95	−30.6719	−1.5227	−0.19492
21	−260.557	−17.3158	1.04907	0.203563
41	−272.87	−3.88662	1.42637	0.202969
61	−287.108	7.75418	1.20409	0.102103
81	−303.476	17.1166	2.08415	0.140983
101	−322.092	20.0399	5.62498	0.441927
121	−342.555	2.72008	12.2203	0.865238
141	−363.052	−60.973	18.0403	0.693823
161	−379.526	−194.414	9.12321	−1.73959
181	−387.473	−352.952	−43.9436	−8.68316
201	−30.7714	−335.131	−48.0968	−5.8236
221	−9.52	−206.144	9.24006	4.61105
241	2.34041	−57.7983	21.2462	5.31763
261	4.73915	17.2032	12.6207	2.49536
281	2.62052	27.1301	2.63466	0.175311
301	0.302986	11.9368	−1.6725	−0.57083
321	−0.56575	−0.29132	−1.55673	−0.35908
341	−0.36263	−2.93506	−0.33357	−2.65E-02
361	1.01E-02	−0.99446	0.207692	7.57E-02
381	8.10E-02	0.530845	0.120074	2.88E-02

References

[1] J. Heyman, The Stone Skeleton: Structural Engineering of Masonry Architecture, 1995.

[2] E. Bernat-Maso, L. Gil e, J. Marcé-Nogué, «The structural performance of arches made of few vossoirs with dry-joints, Struct. Eng. Mech. 44 (2012) 775–799.

[3] D. Aita e, A. Sinopoli, «Revisiting monasterio's unpublished manuscript: a critical review of the collapse modes analysis of non-symmetric and symmetric masonry arches, Int. J. Architect. Herit. 14 (2020) 762–793.
[4] G. Cocchetti e E. Rizzi, «Analytical and numerical analysis on the collapse modes of least-thickness circular masonry arches at decreasing friction, Frat. Ed. Integrità Strutt. 14 (2020) 356–375.
[5] M. Pepe, M. Sangirardi, E. Reccia, M. Pingaro, P. Trovalusci, e G. de Felice, «Discrete and continuous approaches for the failure analysis of masonry structures subjected to settlements, » Frontiers in Built Environment 6 (2020).
[6] M. Gilbert, C. Casapulla e, H.M. Ahmed, «Limit analysis of masonry block structures with non-associative frictional joints using linear programming, Comput. Struct. 84 (2006) 873–887.
[7] G. Maier, Shakedown theory in perfect elastoplacity with associated and nonassociated flow-laws: A finite element, linear programming approach, Meccanica 4 (3) (1969) 250–260.
[8] S. Palladino, L. Esposito, P. Ferla, E. Totaro, R. Zona, V. Minutolo, Experimental and numerical evaluation of residual displacement and ductility in ratcheting shakedown of an aluminium beam, Appl. Sci. 10 (10) (2020).
[9] F. Vincenzo, An approach to the limit design of masonry arches under seismic loads, in: Plasticiy Today, 1985, pp. 821–834. London.
[10] M. Breccolotti, L. Severini, N. Cavalagli, F.M. Bonfigli, e V. Gusella, «Rapid evaluation of in-plane seismic capacity of masonry arch bridges through limit analysis, » Earthquake and Structures 15 (2018) 541–553.
[11] G. Tempesta, e S. Galassi, «Safety evaluation of masonry arches. A numerical procedure based on the thrust line closest to the geometrical axis, Int. J. Mech. Sci. 155 (2019) 206–221.
[12] S. Coccia, F. Di Carlo, e G. Forino, «Strength of cracked masonry buttresses under horizontal loads, in: Brick and Block Masonry: Trends, Innovations and Challenges - Proceedings of the 16th International Brick and Block Masonry Conference, IBMAC, 2016, 2016.
[13] N. Grillanda, M. Valente, G. Milani, A. Chiozzi, A. Tralli, Advanced numerical strategies for seismic assessment of historical masonry aggregates, Eng. Struct. 212 (2020).
[14] N. Grillanda, A. Chiozzi, G. Milani, A. Tralli, Collapse behavior of masonry domes under seismic loads: An adaptive NURBS kinematic limit analysis approach, Eng. Struct. 200 (2019).
[15] P. Block, T. Ciblac e, J. Ochsendorf, «Real-time limit analysis of vaulted masonry buildings, Comput. Struct. 84 (2006) 1841–1852.
[16] A. Romano e, J.A. Ochsendorf, «The mechanics of Gothic masonry arches, Int. J. Architect. Herit. 4 (2010) 59–82.
[17] P. Zampieri, F. Faleschini, M.A. Zanini, e N. Simoncello, «Collapse mechanisms of masonry arches with settled springing, Eng. Struct. 156 (2018) 363–374.
[18] S. Galassi, G. Misseri, L. Rovero, e G. Tempesta, «Failure modes prediction of masonry voussoir arches on moving supports, Eng. Struct. 173 (2018) 706–717.
[19] S. Coccia, F. Di Carlo, e Z. Rinaldi, «Collapse displacements for a mechanism of spreading-induced supports in a masonry arch, » International Journal of Advanced Structural Engineering 7 (2015) 307–320.
[20] F. Di Carlo, S. Coccia e Z. Rinaldi, «Collapse load of a masonry arch after actual displacements of the supports, Arch. Appl. Mech. 88 (2018) 1545–1558.
[21] F. Portioli, e L. Cascini, «Large displacement analysis of dry-jointed masonry structures subjected to settlements using rigid block modelling, Eng. Struct. 148 (2017) 485–496.
[22] L. Cascini, R. Gagliardo e, F. Portioli, «LiABlock_3D: a software tool for collapse mechanism analysis of historic masonry structures, Int. J. Architect. Herit. 14 (2020) 75–94.
[23] G. Lengyel, e K. Bagi, «Horizontal reaction components of pointed vaults,» 1 (2016) 398–420.
[24] H. Alexakis e, N. Makris, «Limit equilibrium analysis of masonry arches, Arch. Appl. Mech. 85 (9–10) (9 2015) 1363–1381.
[25] H. Alexakis e, N. Makris, «Minimum thickness of elliptical masonry arches, Acta Mech. 224 (12) (12 2013) 2977–2991.
[26] D. Aita, R. Barsotti, e S. Bennati, «Equilibrium of pointed, circular, and elliptical masonry arches bearing vertical walls, J. Struct. Eng. 138 (2012) 880–888.
[27] R. Zona, L. Esposito, P. Ferla, S. Palladino, E. Totaro, e V. Minutolo, «Lower bound limit analysis of parabolic domes based on spherical analytical solution, Int. J. Adv. Res. Eng. Technol. 11 (2020) 59–79.
[28] S. Timoshenko e S. Woinowsky-Krieger, Theory of Plates and Shells.
[29] D.C. Drucker, «A definition of a stable inelastic material, J. Appl. Mech. 26 (1959) 101–195.
[30] S. Wolfram, The Mathematica® Book, 4th, a cura di, Wolfram Media, 1999, p. 1470.